The CaFe Experiment:

Proton Pairing Mechanisms in Heavy Nuclei

Proposal PR12-16-XXX to Jefferson Lab PAC 44, July 2016

C.E. Hyde, L.B. Weinstein (co-spokesperson)
Old Dominion University, Norfolk VA

E. Cohen (co-spokesperson), M. Duer, E. Piasetzky
Tel-Aviv University, Tel Aviv, Israel

S. Gilad, O. Hen (co-spokesperson), A Papadopoulou, A. Schmidt, B.A. Schmookler, E. Segurra, and R.C. Torres
Massachusetts Institute of Technology, Cambridge, MA

D.W. Higinbotham
Thomas Jefferson National Accelerator Facility, Newport News, VA

A. Beck, I Korover, and S. Maytal-Beck
Nuclear Research Center Negev, Beer-Sheva, Israel

(Dated: May 23, 2016)

Nucleon-nucleon short range correlated (NN SRC) pairs account for about 25% of nucleons in medium to heavy nuclei and about 75% of their kinetic energy. Almost all high-momentum protons in nuclei have a correlated partner and that partner is almost always a neutron.

While the general outline of nucleon pairing is explained by the nucleon-nucleon tensor force, we still do not understand quantitatively the details of that pairing. In order to study this, we plan to measure how the number of high-momentum protons in the nucleus changes when we dramatically increase the number of neutrons or the number of protons and neutrons in the nucleus.

We propose to measure the relative probability of finding high-momentum ($p > p_{fermi}$) and low momentum ($p < p_{fermi}$) protons in ^{40}Ca, ^{48}Ca, and ^{54}Fe. We will measure how this probability changes from ^{40}Ca, a symmetric nucleus, to ^{48}Ca with 8 more neutrons, and to ^{54}Fe, with 8 more neutrons and 6 more protons. The eight extra neutrons in ^{48}Ca constitute a 40% increase in the neutron number. These eight neutrons are in the $1f_{7/2}$ shell, outside the ^{40}Ca closed shell, and are thus in very different orbitals from the protons they are expected to pair with.

We will measure $A(e, e'p)$ cross sections and extract the probabilities of finding high and low missing-momentum protons from these cross sections. We will measure these cross sections at high Q^2 and $x > 1$ to reduce the effects of Meson Exchange Currents and Isobar Currents, and at non-perpendicular kinematics to reduce the effects of Final State Interactions. We will use an 11 GeV beam and detect the scattered electron in the SHMS and the knocked out proton in the HMS.

The double ratios of high and low missing momentum protons in different nuclei will correspond to the relative probabilities for protons to belong to SRC pairs in those nuclei. We will compare these double ratios to different models of proton pairing.

This measure will significantly improve our quantitative understanding of nucleon pairing in nuclei.

We request XXX (between 2 and 5) days of beam time in Hall C for the measurements of ^{40}Ca, ^{48}Ca, and ^{54}Fe$(e, e'p)$.

I. INTRODUCTION AND MOTIVATION

A. Short Range Correlated NN Pairs in Nuclei

The mean field approximation describes bulk properties of nuclei, such as shell structure, excitation energies, and spins remarkably well; however, only about 70% of nucleons occupy mean field orbitals [1, 2]. Describing the dynamics of the remaining nucleons is a major challenge facing nuclear physics today.

The Jefferson Lab 6 GeV program made tremendous progress in understanding these remaining nucleons. Results from inclusive (e, e') measurements at $x = Q^2/2m\nu > 1$ (see Section I D for variable definitions) indicate that the nucleon momentum distributions in all nuclei are remarkably similar for $p > 275$ MeV/c [3–5]. About 25% of nucleons in medium to heavy nuclei have momentum greater than the typical mean-field (Fermi) momentum, $p > p_{fermi}$ where $p_{fermi} \approx 250$ MeV/c [4, 5]. Exclusive $(e, e'pN)$ measurements show that in the symmetric ^{4}He and ^{12}C nuclei, almost every proton with momentum $300 < k < 600$ MeV/c has a correlated partner nucleon, with neutron-proton (np) pairs outnumbering proton-proton (pp) and, by inference, neutron-neutron (nn) pairs by a factor of ≈ 20 [6–8]. In asymmetric heavy nuclei with unequal numbers of the different fermions, high-momentum protons still disproportionately belong to np pairs [9]. The observed np-SRC dominance in heavy nuclei is a non-trivial result since in these heavy nuclei, nucleons from different shells could create $l \neq 0$ pp and nn pairs with non-zero spin that are also sensitive to the tensor part of the NN-interaction, thereby diminishing the observed np dominance observed in light nuclei. Two of these results were published in *Science*.

The observed np-SRC pair dominance also implies that in heavy neutron-rich nuclei the high-momentum tail contains the same amount of neutrons and protons, leaving the excess neutrons to occupy low-momentum states (see Fig. 1). This leads to a possible inversion of momentum sharing between protons and neutrons where protons (i.e. the minority) have larger average momentum. This inversion should be universal for two-component Fermi systems with a short-range interaction between the different Fermions.

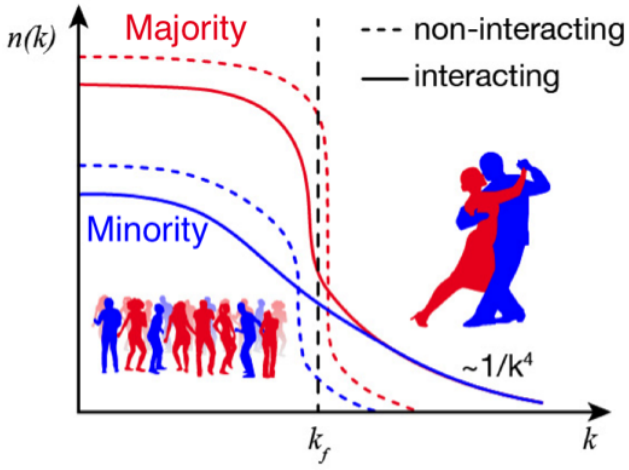

FIG. 1: A schematic representation of the main characteristics of the momentum distribution, $n(k)$, of asymmetric nuclei. The dashed lines show the standard non-interacting system while the solid lines show the effect of including a short-range interaction between different Fermions which creates a high-momentum ($k > k_F$) tail. This is analogous to a dance party with a majority of girls, where boy-girl interactions will make the average boy dance more than the average girl, and hence the boys will have larger average momentum [9].

B. Implications of momentum sharing in imbalanced Fermi systems

The *np*-dominance of SRC pairs and the resulting inversion of the momentum sharing in heavy neutron-rich imbalanced nuclei have wide ranging implications in astro, nuclear and particle physics. These include the determination of the density dependence of the nuclear symmetry-energy up to supra-nuclear densities [10–15], analysis of neutrino-nucleus scattering data for the determination of the nature of the electro-weak interaction [16, 17], the quark structure of bound nucleons through the EMC effect [18, 19], the isospin dependence of the EMC effect as a cause of the standard-model NuTeV anomaly [18, 20–23], double-beta decay matrix elements [24], neutron star equation of state and cooling rates [25], the universality of contact interactions in Fermi systems [26], etc.

1. Neutrino-nucleus scattering

One application of SRCs is in neutrino physics where most experiments still use a simple relativistic Fermi gas model to describe the nucleus. Recent high precision measurements of charged current quasi-elastic neutrino-nucleus scattering cross-sections [16, 17] show the need to include the effects of *np*-SRC pairs in both their reaction model and detector response.

This is expected to be a crucial ingredient in facilitating the precision requirements of next generation neutrino experiments [27]. This proposed experiment will help us understand precisely which nucleons form SRC pairs, which in turn will improve our understanding of neutrino-nucleus interactions. In this way, these proposed measurements will complement experiment E12-14-012, which has been approved to extract the spectral function (i.e., the single-nucleon properties) of ^{40}Ar.

2. The EMC effect and the NuTeV anomaly

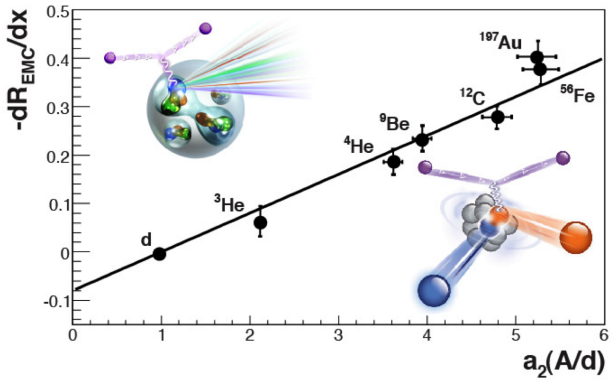

FIG. 2: The strength of the EMC effect plotted vs the relative probability of a nucleon to belong to an SRC pair for a variety of nculei. See Refs. [18, 19] for details.

The deep inelastic scattering cross section for scattering from bound nucleons differs from that of free nucleons. This phenomenon, first discovered 30 years ago, is known as the EMC effect, and its origin is still not fully understood [28–32]. The EMC effect implies modification of bound nucleon structure [32] and its size is linearly correlated with the number of SRC (high momentum) pairs in nuclei (see Fig. 2) [18, 19]. This implies the possibility that both stem from high momentum (i.e., large virtuality) nucleons in the nucleus. Two 12-GeV experiments will measure deep inelastic scattering (DIS) off one nucleon in the deuteron by detecting (tagging) the high-momentum backward-angle spectator protons [33] or neutrons [34]. By measuring the nucleon-momentum dependence of the bound nucleon structure functions, these experiments will determine whether the EMC effect is due to a small modification of the large number of mean-field nucleons or a large modification of the smaller number of SRC nucleons.

Theoretical calculations show that an isospin dependent EMC effect in neutron-rich nuclei, and in particular iron, could explain the NuTeV anomaly [23]. The latter is a three standard deviation difference from the Standard Model prediction in the measurement of

the electroweak-mixing (Weinberg) angle using neutrino scattering from iron [22]. One original model employed a mean-field model to explain the possible existence of such an isospin dependent result. Alternatively, if the EMC nucleon modification is dominated by high momentum nucleons and protons have higher average momentum than neutrons in $N > Z$ nuclei, then this would provide an alternative model for an isospin dependent EMC effect which could quantitatively explain the NuTeV anomaly. By studying how changing the number of protons and neutrons affects the number of high momentum protons, our proposed measurement will provide input to calculations of the NuTeV anomaly.

3. The nuclear symmetry energy

The nuclear symmetry energy describes how the energy per nucleon in nuclear matter changes as a function of the proton fraction. While its value at the nuclear saturation density is relatively well constrained [14], its density dependence is not, largely due to uncertainties in the tensor component of the nucleon-nucleon interaction [12, 13]. Knowledge of this density dependence at supra-nuclear densities is important for different aspects of nuclear astrophysics and in particular neutron stars [14]. Recent calculations show that the inclusion of high-momentum tails, dominated by tensor force induced *np*-SRC pairs, dramatically softens the nuclear symmetry energy at supra-nuclear densities [10–13]. Including these high-momentum tails decreases the kinetic part of the nuclear symmetry energy at nuclear density from the free Fermi Gas Model value of +12.5 MeV to −10 MeV, increasing the potential part at saturation density and softening its density dependence [15]. Measuring the change in the average proton momentum (and hence, kinetic energy) as we change the number of neutrons and protons will help us refine this calculation.

4. Cooling rates of neutron stars

Theoretical analysis of neutrino cooling data indicates that neutron stars contain about 5 to 10% protons and electrons in the crust. Calculations show that *np*-dominance of SRC pairs in asymmetric nuclei and nuclear matter can bring a large fraction of the protons above their Fermi momentum, opening holes below the Fermi momentum. The existence of such fast protons and the resulting holes in the Fermi sphere might allow for some direct, rather

than modified, Urca cooling of neutron stars, even below threshold [25]. Since direct Urca cooling is about 10^6 times faster than modified Urca cooling, small changes could have a disproportionate impact on the cooling rate and the star lifetime.

New, high-precision, data on the dynamics of 2N-SRC pairs in heavy nuclei and their dependence on the nuclear asymmetry will improve the accuracy and increase the reliability of such calculations.

5. *Ultra-cold interacting Fermi Systems*

Two-component many-body Fermi systems with a short-range interaction that is strong between different Fermions and weak between Fermions of the same type have several universal features [35] including the existence of a high-momentum tail ($k > k_F$) that scales as $n(k) = Ck^{-4}$ and is dominated by short-range correlated (SRC) pairs of different Fermions. The scale factor, C, is known as Tan's contact and describes the thermodynamics of the system.

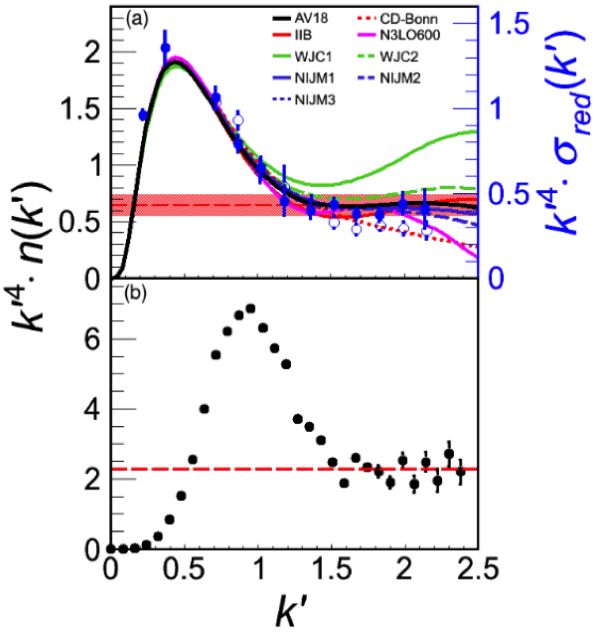

FIG. 3: The scaled momentum distribution, $k^4 n(k)$ in units of k_F, for nuclear (top) and atomic (bottom) systems. Bottom: The measured momentum distribution of ^{40}K atoms in a symmetric two-spin state ultra-cold gas with a short-range interaction between the different spin-states [36]. Top: The proton momentum distribution in deuterium calculated with state-of-the-art nucleon-nucleon potentials (solid lines) and the extracted from $d(e, e'p)$ cross-section measurements (blue points). The dashed lines are the results of a fit to a constant at $k > 1.5k_F$. See Ref. [26] for details.

The high-momentum tail and the thermodynamical Tan relations were experimentally verified in two-spin state ultra-cold atomic gases [36]. Fig. 3 shows the scaled momentum distribution, $k^4 n(k)$ in units of k_F, of ^{40}K atoms in ultra-cold balanced two-spin state atomic gas (bottom) [36] and of nucleons bound in deuterium (top) [26]. The deuteron momentum distribution is calculated using state-of-the-art nucleon-nucleon potentials and extracted

from $d(e,e'p)$ measurements. Both distributions have the same normalization for $n(k)$. The momentum distribution in both systems scales as k^{-4} starting at $k \approx 1.5k_F$ [26].

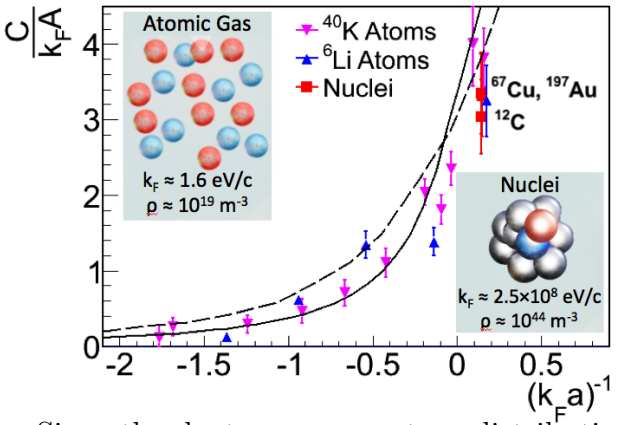

FIG. 4: The pairing probability, C, as a function of the dimensionless interaction strength for atomic and nuclear systems. See Ref. [26] for details.

Since the deuteron momentum distribution is proportional to k^{-4} and the nuclear momentum distributions at $k > 275$ MeV/c are proportional to the deuteron's [3–5], the momentum distribution for all nuclei scales as k^{-4} for $k > 275$ MeV/c. Fig. 4 shows the pairing probability, known as the Contact, for nuclear and atomic systems as a function of their dimensionless interaction strength. Despite at least a 20 order-of-magnitude difference in density, the atomic and nuclear systems have the same pairing probability for the same interaction strength.

A detailed study of the np-dominance of SRC pairs in heavy nuclei and its dependence on the nuclear asymmetry will allow a further study of the connection between Tan's universal relations, nuclei, and nuclear matter.

C. Nucleon pairing mechanisms

We know from previous measurements that almost all high momentum nucleons in nuclei belong to SRC NN pairs and that these pairs are predominantly np pairs, even in heavy asymmetric nuclei such as lead. We also know that this unlike-fermion pairing is similar to pairing in two-component ultra-cold atomic gases. This pairing could also invert the average momentum in asymmetric nuclei, giving the minority nucleons more average momentum than the majority. However, we do not know the details of this pairing mechanism.

E08-014 measured the per-nucleon ratio of (e,e') cross sections for ^{48}Ca to ^{40}Ca at $1.25 \leq Q^2 \leq 2$ GeV^2 [37]. If SRC is independent of isospin (i.e., due to all possible nn, np and pp

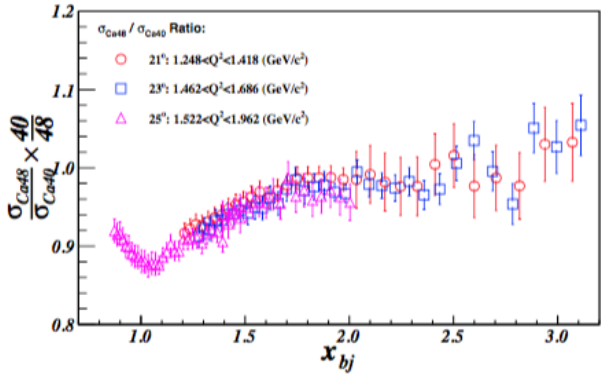

FIG. 5: The per-nucleon (e, e') cross section ratio of ^{48}Ca to ^{40}Ca. The ratio in the scaling region ($1.7 < x < 2$ for $Q^2 \approx 1.3$ and $1.5 < x < 2$ for $Q^2 \approx 2$ GeV^2) is about 0.97 [37].

pairs), then the cross section for scattering from one nucleon in an SRC pair is

$$\sigma \propto 2\sigma_{ep}(Z(Z-1)/2) + (\sigma_{ep} + \sigma_{en})(NZ) + 2\sigma_{en}(N(N-1)/2) \quad . \tag{1}$$

At the E08-014 measured momentum transfer, $\sigma_{ep} \approx 3\sigma_{en}$. Thus, for isospin independent SRC, the per-nucleon cross section ratio of ^{48}Ca to ^{40}Ca should be 1.10. On the other hand, if SRC are dominated by np pairs and we apply simple pair counting (e.g., NZ), then the expected ratio of ^{48}Ca to ^{40}Ca would be 1.17. These predictions are very similar and difficult to distinguish experimentally. However, the measured per-nucleon cross section ratio is about 0.97, disagreeing with both simple predictions (see Fig. 5). A more sophisticated calculation counting the number of NN pairs in a nodeless relative S-state [38–40] predicted a ratio of 0.99. This is discussed in more detail below.

Exact calculations of nuclear wave functions are only possible for relatively light nuclei, up to approximately ^{12}C [41]. They find that np pairs dominate at high relative momentum ($300 \leq p_{rel} \leq 600$ MeV/c) (see Fig. 6). Even in ^{8}He, where combinatorially there are more nn pairs than np pairs, the momentum density of the np pairs is greater than the nn pairs at $p_{rel} > 200$ MeV/c. This is one more example of the failure of simple pair-counting combinatorics.

Ryckebusch, Cosyn and collaborators [40] have calculated single-nucleon momentum distributions in heavier nuclei by shifting the complexity induced by SRC from the wave functions to the operators. They find that the SRC-related high momentum tail of the single-nucleon momentum distribution is dominated by correlation operators acting on mean-field pairs with zero relative radial and angular momentum quantum numbers ($n = 0, l = 0$).

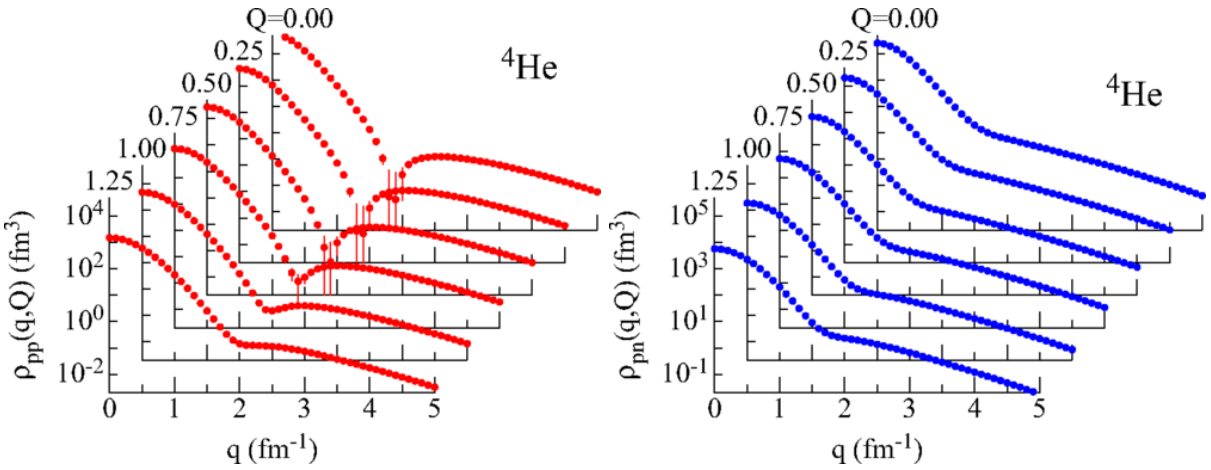

FIG. 6: The proton-proton (left) and proton-neutron (right) momentum distribution in ^{4}He averaged over the directions of the relative ($\vec{q}$) and total ($\vec{Q}$) pair momenta as a function of q for several fixed values of Q from 0 to 1.25 fm^{-1} [41].

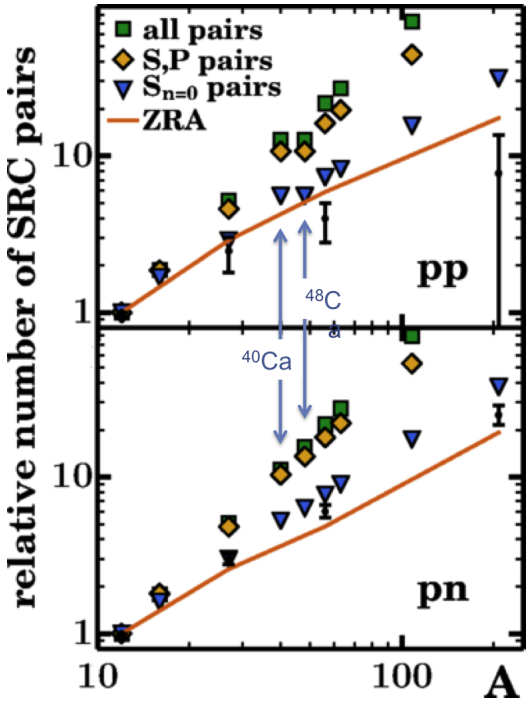

FIG. 7: Mass dependence of the number of pp (top panel) and pn (bottom panel) SRC pairs of nucleus A relative to ^{12}C . Data (small black circles with error bars) are extracted from the measured CLAS $A(e,e'p)$ and $A(e,e'pp)$ cross-section ratios [9, 21] after correcting for FSI. The green squares correspond with unconditional counting of the pp pairs ($Z(Z-1)/30$) and pn pairs ($ZN/36$) for ^{12}C, ^{16}O, ^{27}Al, ^{40}Ca, ^{48}Ca, ^{56}Fe, ^{63}Cu, ^{108}Ag, and ^{208}Pb. The yellow diamonds are the ratios obtained by counting independent particle model (IPM) pairs in relative S or P states. The blue triangles count IPM ($l=0, n=0$) pairs. The solid line denotes the result of a reaction-model calculation for scattering from close-proximity (zero-range) pairs which takes full account of the experimental phase space [42].

Using this method, we calculated the expected number of NN SRC pairs in nuclei from carbon to lead and compared that to the experimentally extracted number of pn and pp pairs in those nuclei [38, 39, 42]. The measured number of pp and pn pairs increases far more slowly than simple combinatorics ($Z(Z-1)/2$ and NZ respectively) and is much more consistent with the number of NN pairs with $n=0, l=0$ (see Fig. 7) [42]. Note that the number of pp pairs is the same for ^{40}Ca and ^{48}Ca, while the number of pn pairs increases

steadily from ^{40}Ca to ^{48}Ca to ^{56}Fe. This implies that adding neutrons to ^{40}Ca increases the number (and hence the proportion) of high momentum protons and that adding protons to ^{48}Ca increases the number, but not the proportion of high momentum protons.

1. NN pairing in ^{40}Ca, ^{48}Ca, and ^{54}Fe

Since high-momentum protons in the nucleus almost entirely come from SRC NN pairs, we will use the number of detected high-momentum protons as a measure of the number of SRC pairs in a given nucleus. We expect these pairs to be predominantly np pairs.

We propose to measure the relative proportion of high-momentum protons in ^{40}Ca, ^{48}Ca, and ^{54}Fe to test pairing mechanisms. ^{40}Ca and ^{48}Ca are both doubly closed-shell nuclei. ^{40}Ca has filled proton and neutron $1s, 1p$, and $2s/1d$ shells. ^{48}Ca has, in addition, eight more neutrons in the $1f_{7/2}$ shell. Somehow these extra $1f_{7/2}$ neutrons form SRC pairs with the 40 nucleons in the inner core. This pairing is non-trivial.

By measuring the relative number of high-momentum protons in ^{40}Ca and ^{48}Ca nuclei, we can directly measure the extra number of cross-shell np pairs caused by adding eight $1f_{7/2}$ neutrons.

Similarly, by adding six $1f_{7/2}$ protons to ^{48}Ca, we get ^{54}Fe. These extra protons can pair with any of the 40 nucleons in the inner shells or with the eight neutrons in the $1f_{7/2}$ shell. Thus, measuring the difference between ^{40}Ca and ^{48}Ca will teach us about the pairing of protons and neutrons from different shells and measuring the difference between ^{48}Ca and ^{54}Fe will teach us about the pairing of protons and neutrons from both different shells and the same shell.

We can predict the number of high momentum protons in the different nuclei in several different models:

1. isospin independence so that the the number of high momentum protons is proportional to the number of protons,

2. isospin-independent pair dominance with np, pp, and nn combinatorial pairs (see Eq. 1),

3. np pair dominance with combinatorial pairs (NZ),

4. np pair dominance with all relative S and P pairs and

Model	^{40}Ca	^{48}Ca	^{54}Fe	^{48}Ca/^{40}Ca	^{54}Fe/^{48}Ca	^{54}Fe/^{40}Ca
1 – all protons	20	20	26	1	1.3	1.3
2 – all pairs	2740	3380	4862	1.23	1.44	1.77
3 – all np pairs	400	560	728	1.4	1.3	1.8
4 – S and P np pairs						
5 – $l = 0, n = 0$ np pairs	6	7.2	8.8	1.2	1.2	1.5

TABLE I: The expected number of high-momentum protons for each of the five models listed. See text for description of models. Note that the values for models 4 and 5 use ^{56}Fe rather ^{54}Fe. **we need to somehow make this either expected number or make all numbers relative to 40Ca**

5. np pair dominance with only relative $n = 0, l = 0$ pairs.

The relative number of high-momentum protons for each of the five models is shown in Table I.

D. Formalism

The cross section for electron-induced proton knockout from nuclei $A(e, e'p)$ can be written (assuming factorization) as:

$$\frac{d^6\sigma}{d\nu dE_{miss} d\Omega_e d\Omega_p} = K\sigma_{ep} S^D(E_{miss}, p_{miss})$$

where E and E' are the initial and scattered electron energies, $\vec{p}_e$ and $\vec{p}'_e$ are the initial and scattered electron momenta, $\vec{p}_p$ is the outgoing proton momentum, and Ω_e and Ω_p are the electron and proton solid angles respectively. The energy transfer $\nu = E - E'$, the momentum transfer $\vec{q} = \vec{p}_e - \vec{p}'_e$, four-momentum transfer squared $Q^2 = \vec{q}^2 - \nu^2$, and the Bjorken scaling variable $x = Q^2/2m\nu$. The missing energy and missing momentum are

$$E_{miss} = \nu - T_p - T_{A-1} \quad (2)$$

$$\vec{p}_{miss} = \vec{q} - \vec{p}_p \quad (3)$$

where T_p and T_{A-1} are the kinetic energies of the outgoing proton and residual nucleus. The kinematic factor is

$$K = \frac{E_p p_p}{(2\pi)^3},$$

σ_{ep} is cross section for scattering an electron from a bound proton, and $S^D(E_{miss}, p_{miss})$ is the distorted spectral function. In the absence of final state interactions (FSI), S is the probability to find a nucleon in the nucleus with separation energy E_{miss} and momentum p_{miss} [43].

We plan to extract the distorted spectral function from the measured cross sections:

$$S^D(E_{miss}, p_{miss}) = \left(\frac{1}{K\sigma_{ep}}\right) \frac{d^6\sigma}{d\nu dE_{miss} d\Omega_e d\Omega_p} \tag{4}$$

and then correct it for the effects of FSI.

For each nucleus we plan to measure at one low-p_{miss} kinematics and one high-p_{miss} kinematics. We will correct the distorted spectral function for FSI. For each value of missing momentum we will only detect protons covering a fraction $f(p_{miss})$ of the 4π solid angle available to $\vec{p}_{miss}$. We will further correct our measurement by $1/f$ to account for this. We will then integrate the corrected distorted spectral functions over missing energy and missing momentum. The relative amount of high-momentum protons in each nucleus will equal the ratio of the integrated distorted spectral functions at high-p_{miss} and low-p_{miss}.

The double ratio of the integrated distorted spectral functions at high-p_{miss} and low-$p_{miss}$for different nuclei should correspond to the ratios in the last three columns of Table I.

The correction, $1/f$, for the undetected protons is purely geometrical. It is easy to calculate and will also cancel in the double ratio of high-p_{miss} and low-p_{miss} for different nuclei.

There are a number of uncertainties in the extraction of the distorted spectral function, including the validity of factorization, the off-shell extrapolation of the electron-proton cross section, and the effects of FSI. Over the limited acceptance of the spectrometers, factorization should be accurate to about 10% and the effects of factorization should cancel almost completely when calculating cross section ratios. Similarly, while there are several different off-shell prescriptions for the electron-proton cross section [44], the effects of these will also cancel when calculating ratios at similar p_{miss}. The effect of FSI is discussed in section I E.

E. Final State Interactions

We want to extract the

- ratios of high to low momentum protons in each of ^{40}Ca, ^{48}Ca, and ^{54}Fe,
- ratios of high-momentum protons in ^{40}Ca to ^{48}Ca and in ^{54}Fe to ^{48}Ca, and
- double ratios of high to low momentum protons in ^{40}Ca relative to ^{48}Ca, and in ^{54}Fe relative to ^{48}Ca.

We will need to correct each of these ratios for the effects of final state interactions (FSI).

There are two general effects from rescattering of the outgoing proton: a shift in momentum due to the real part of the proton-nucleus potential, and rescattering of the proton that changes its momentum and potentially knocks out a second nucleon. Loss of protons from a particular kinematic bin can be calculated accurately in the Glauber approximation for high momentum protons. Rescattering of protons into a particular kinematic bin is harder to calculate.

We will measure the $(e, e'p)$ reaction at $\theta_{rq} \leq 40^\circ$ to significantly reduce contributions from nucleon rescattering.

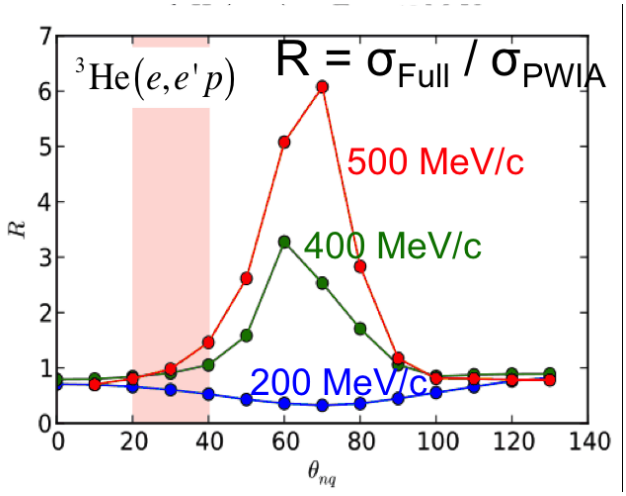

FIG. 8: The calculated ^{3}He$(e, e'p)$ ratio of the cross section which includes rescattering of the struck nucleon (FSI) to the PWIA cross section for $p_{miss} = 0.2$ (blue), 0.4 (green), and 0.5 (red) GeV/c as a function of θ_{rq}, the angle between the recoil momentum and $\vec{q}$ in the laboratory frame [45]. The tan band indicates the angles for the measurements proposed here.

This rescattering of protons *into* a particular kinematic bin is maximum at perpendicular kinematics, where the angle between the recoil momentum and the momentum transfer,

$\theta_{rq} \approx 70°$. This happens because most collisions between high-momentum protons and other nucleons in the nucleus deflect the high-momentum only slightly, kicking the struck nucleon out at about 70° (non-relativistically it would be about 90°). This can be seen clearly in calculations of the data of [46], where the cross section at $p_{miss} > 250$ MeV/c and $E_{miss} \approx p_{miss}^2/2m$ is due almost entirely to rescattering. Calculations by Sargsian [45] for ^{3}He$(e, e'p)$ show very large contributions due to proton rescattering peaked at $\theta_{rq} \approx 70°$. In order to avoid these regions where rescattering is much larger than the SRC signal, we will choose $\theta_{rq} \leq 40°$.

We will calculate the rescattering of protons *out* of our kinematic bins using the Glauber approximation. Glauber calculations have been shown to reproduce nucleon transparency measurements in nuclei [47]. In addition, since we are primarily interested in the relative proportions of high- and low-initial-momentum protons in the different nuclei, we are primarily sensitive to the *difference* in the transparency from ^{40}Ca to ^{54}Fe. The measured transparency in ^{56}Fe at $Q^2 = 3.3$ GeV^2 is $T = 0.4$ [48]. The calculated transparency for knocked-out protons at $Q^2 = 2.4$ GeV^2 and $50 \leq p_{miss} \leq 150$ MeV/c (i.e., for kinematics similar to our proposed kinematics) is about $T = 0.43, 0.37$, and 0.36 for ^{40}Ca, ^{48}Ca, and ^{54}Fe, respectively. This difference is consistent with the expected variation of the opacity (equals one minus the transparency) as $A^{1/3}$.

For a given nucleus, protons with large and small p_{miss} have the same measured transparency [47]. Therefore the ratio of the large p_{miss} to small p_{miss} cross sections for a given nucleus should be independent of FSI.

The ratios of high-momentum protons in ^{40}Ca to ^{48}Ca and in ^{54}Fe to ^{48}Ca will need to be corrected for FSI. We will calculate the small change in the transparency from ^{54}Fe to ^{48}Ca and from ^{48}Ca to ^{40}Ca and compensate the data for it. In addition, we will construct an artificial, approximately $N = Z$ nucleus by averaging the results for ^{40}Ca and ^{54}Fe. Since the transparency of (^{40}Ca+^{54}Fe)/2 and ^{48}Ca should be very similar, the ratio of high momentum protons in (^{40}Ca + ^{54}Fe)/2 to ^{48}Ca should be almost independent of FSI.

F. Impact on the 12 GeV JLab program

The results of this proposed measurement will complement other 12 GeV JLab experiments, particularly measurements of the spectral function of ^{40}Ar, inclusive quasielastic

(e, e') measurements of nuclei at $x > 1$, and inclusive deep inelastic (e, e') measurements of nuclei at $x < 1$.

E12-14-012 will measure electro-induced proton knockout from ^{40}Ar (or possibly ^{40}Ti) to extract its spectral function (i.e., its single-nucleon properties). They will measure the missing momentum distribution of the cross section for the different mean-field orbitals in argon ($1s_{1/2}, 2s_{1/2}, 1p_{1/2}, 1p_{3/2}, 1d_{3/2}$ and $1d_{5/2}$). Our measurement will focus instead on the knockout of high-momentum protons belonging to short range correlated pairs, studying how their number changes when we change the number of neutrons and then the number of protons in the nucleus. Our measurement of SRC protons will thus complement E12-14-012's measurement of mean-field protons.

E12-06-105 will measure inclusive electron scattering (e, e') on a wide variety of nuclei at $1.4 < x$ and $Q^2 \leq 5$ GeV^2 to extend previous studies of short range correlations in few-body and heavy nuclei. However, inclusive cross section measurements cannot distinguish between electron scattering from a proton or from a neutron and thus cannot distinguish between *pp* and *pn* SRC pairs. By studying how the number of high-momentum protons changes when we change the number of neutrons and then the number of protons in the nucleus, our experiment will provide complementary information.

E12-10-108 will measure the EMC effect in inclusive deep inelastic (e, e') measurements of nuclei at $x < 1$. By comparing their measurements of the EMC effect to the SRC ratios measured at $x > 1.4$ in E12-06-105, they will extend our understanding of the EMC-SRC correlation. By studying the details of proton-neutron pairing, our experiment will provide complementary information that will help us understand how the EMC effect and SRC ratios change from ^{40}Ca to ^{48}Ca.

G. Previous Measurements

While there have been a number of $(e, e'p)$ experiments at Jefferson Lab [46, 48–59], they have almost all focussed on measuring nuclear transparencies or single nucleon properties of nuclei (i.e., nucleon knockout from valence shells). Very few have measured $(e, e'p)$ at SRC kinematics. Some experiments focussed on measuring the correlated partner of the knocked-out proton [6, 8, 60]. However, these experiments measured nucleon knockout from symmetric nuclei (He and C) and were thus insensitive to the effects on the proton

momentum distribution of adding neutrons.

Both Rohe *et al* [57] and Benmokhtar *et al* [46] measured $(e, e'p)$ over a wide range of missing energy and missing momentum to look for the effects of correlations. Benmokhtar measured the ^{3}He$(e, e'p)$ cross section in perpendicular kinematics (where the missing momentum and hence the undetected nucleon is perpendicular to the momentum transfer) and thus their cross sections in the correlations region are dominated by nucleon rescattering. Rohe *et al.* extracted the nuclear spectral function as a function of E_{miss} for three different values of p_{miss} in parallel kinematics [57]. They compared the measured spectral function to calculations, finding reasonable agreement only at $p_{miss} \approx 250$ MeV/c. They were interested in observing the existence of the correlated part of the spectral function. Our experiment will study in detail how the correlated part changes from ^{40}Ca to ^{48}Ca to ^{54}Fe.

The overall proportion of high momentum nucleons in various nuclei has been extracted from per-nucleon ratios of $A(e, e')$ to $d(e, e')$ cross sections. This has been measured for nuclei from ^{3}He to Au. As shown in Fig. 5 and discussed in Sec. I A, the per-nucleon ratios of ^{48}Ca(e, e') to ^{40}Ca(e, e') cross sections is one. This measurement is sensitive to both high-momentum protons and neutrons in Ca. Our measurement will complement the inclusive (e, e') measurement, since it is only sensitive to protons.

This will be the first $(e, e'p)$ measurement at Jefferson Lab to investigate the effects on nucleon SRC pairing of adding a large number of neutrons and then a large number of protons in medium to heavy nuclei.

II. THE MEASUREMENT

We will measure the $(e, e'p)$ cross section on ^{40}Ca, ^{48}Ca, and ^{54}Fe at high and low missing momentum at large Q^2 and non-perpendicular kinematics. We chose $Q^2 \approx 3$ GeV^2 to minimize the effects of Meson Exchange Currents and Isobar Configurations (Δ production). We chose $\theta_{rq} < 40^\circ$ to minimize the effects of Final State Interactions at large missing momentum. This reduces the energy transfer and thus gives $x = Q^2/2m\nu > 1$, also reducing the effects of MEC and IC.

We will extract the relative probability for a proton to be at high-p_{miss} ($p_{miss} > p_{Fermi} \approx$ 250 MeV/c) by calculating the ratio of the integrated cross section for high-p_{miss} to low-p_{miss} in each of the three nuclei. We will construct several ratios:

- single ratios of high to low momentum protons in each of ^{40}Ca, ^{48}Ca, and ^{54}Fe,
- single ratios of high-momentum protons in ^{40}Ca to ^{48}Ca and in ^{54}Fe to ^{48}Ca, and
- double ratios of high to low momentum protons in ^{40}Ca relative to ^{48}Ca, and in ^{54}Fe relative to ^{48}Ca.

The first and third ratios will be independent of FSI. The second will be corrected for the small change in transparency between ^{40}Ca and ^{54}Fe.

We will use an 11 GeV beam and measure the scattered electron in the SHMS and the knocked out proton in the HMS. The SHMS will operate at a scattering angle of 10°.

A. From cross section to ratios

As described in Section I D, we will measure the $(e, e'p)$ cross section at high- and low-p_{miss} on ^{40}Ca, ^{48}Ca, and ^{54}Fe. We will extract the distorted spectral function using Eq. 4, correct it for the effects of FSI using the Glauber approximation [61], and correct it for the limited p_{miss}-dependent geometrical acceptance. We will then integrate the cross section over missing energy (up to π-emission threshold) and missing momentum. The low-p_{miss} bin will be integrated from 0 to 250 MeV/c and the high-p_{miss} bin will be integrated from about 250 to 500 MeV/c.

We will then construct the ratio of high-p_{miss} to the sum of low- and h-p_{miss} protons for each nucleus. These ratio will give the fraction of high momentum protons, and hence the protons belonging to SRC-pairs in each nucleus. We will compare these single-ratios to calculations of the proportions of high-momentum protons in the different nuclei. The effects of FSI should largely cancel in these ratios.

We will then construct the double ratios of high-p_{miss} to the sum of low- and h-p_{miss} protons for pairs of nuclei. The effects of FSI, ambiguities in the off-shell electron-proton cross section, and the geometrical extrapolation should all cancel in this double ratio. These double ratios should correspond to relative amounts of high-momentum protons in the last three columns of Table I.

[1] L. Lapikas, Nuclear Physics A **553**, 293c (1993).

[2] G. Kramer, H. Blok, and L. Lapiks, Nuclear Physics A **679**, 267 (2001), ISSN 0375-9474, URL http://www.sciencedirect.com/science/article/pii/S03759474000%03791.

[3] K. Egiyan et al. (CLAS Collaboration), Phys. Rev. C **68**, 014313 (2003).

[4] K. Egiyan et al. (CLAS Collaboration), Phys. Rev. Lett. **96**, 082501 (2006).

[5] N. Fomin et al., Phys. Rev. Lett. **108**, 092502 (2012).

[6] R. Subedi et al., Science **320**, 1476 (2008).

[7] E. Piasetzky, M. Sargsian, L. Frankfurt, M. Strikman, and J. W. Watson, Phys. Rev. Lett. **97**, 162504 (2006).

[8] I. Korover, N. Muangma, O. Hen, et al., Phys.Rev.Lett. **113**, 022501 (2014), 1401.6138.

[9] O. Hen et al. (CLAS Collaboration), Science **346**, 614 (2014).

[10] A. Carbone, A. Polls, and A. Rios, Euro. Phys. Lett. **97**, 22001 (2012).

[11] I. Vidaña, A. Polls, and C. m. c. Providência, Phys. Rev. C **84**, 062801 (2011), URL http://link.aps.org/doi/10.1103/PhysRevC.84.062801.

[12] C. Xu, A. Li, and B. Li, J. of Phys: Conference Series **420**, 012190 (2013).

[13] C. Xu and B. Li (2011), 1104:2075.

[14] J. M. Lattimer and Y. Lim, Apj **771**, 51 (2013).

[15] O. Hen, B.-A. Li, W.-J. Guo, L. B. Weinstein, and E. Piasetzky, Phys. Rev. C **91**, 025803 (2015), URL http://link.aps.org/doi/10.1103/PhysRevC.91.025803.

[16] G. A. Fiorentini et al. (MINERvA Collaboration), Phys. Rev. Lett. **111**, 022501 (2013).

[17] G. A. Fiorentini et al. (MINERvA Collaboration), Phys. Rev. Lett. **111**, 022502 (2013).

[18] L. B. Weinstein, E. Piasetzky, D. W. Higinbotham, J. Gomez, O. Hen, and R. Shneor, Phys. Rev. Lett. **106**, 052301 (2011).

[19] O. Hen, E. Piasetzky, and L. B. Weinstein, Phys. Rev. C **85**, 047301 (2012).

[20] L. Frankfurt and M. Strikman, Phys. Rep. **160**, 235 (1988).

[21] O. Hen et al., Int. J. Mod. Phys. E **22**, 133017 (2013).

[22] G. P. Zeller et al., **88**, 091802 (2002).

[23] I. C. Cloët, W. Bentz, and A. W. Thomas, Phys. Rev. Lett. **102**, 252301 (2009), URL http://link.aps.org/doi/10.1103/PhysRevLett.102.252301.

[24] F. Šimkovic, A. Faessler, H. Müther, V. Rodin, and M. Stauf, Phys. Rev. C **79**, 055501 (2009), URL http://link.aps.org/doi/10.1103/PhysRevC.79.055501.

[25] L. Frankfurt, M. Sargsian, and M. Strikman, International Journal of Modern Physics A **23**, 2991 (2008), http://www.worldscientific.com/doi/pdf/10.1142/S0217751X08041207, URL http://www.worldscientific.com/doi/abs/10.1142/S0217751X08041%207.

[26] O. Hen, L. B. Weinstein, E. Piasetzky, G. A. Miller, M. M. Sargsian, and Y. Sagi, Phys. Rev. C **92**, 045205 (2015), URL http://link.aps.org/doi/10.1103/PhysRevC.92.045205.

[27] *"int workshop, neutrino-nucleus interactions for current and next generation neutrino oscillation experiments (int-13-54w).".*

[28] D. Geesaman, K. Saito, and A. Thomas, Ann. Rev. Nucl. and Part. Sci. **45**, 337 (1995).

[29] P. R. Norton, Rep. Prog. Phys. **66**, 1253 (2003).

[30] L. Frankfurt and M. Strikman, Phys. Rev. C **82**, 065203 (2010).

[31] S. A. Kulagin and R. Petti, Nucl. Phys. A **765**, 126 (2006).

[32] S. A. Kulagin and R. Petti, Phys. Rev. C **82**, 054614 (2010).

[33] O. Hen, L. Weinstein, S. Wood, and S. Gilad, *In Medium Nucleon Structure Functions, SRC, and the EMC effect, Jefferson Lab experiment E12-11-107* (2011).

[34] O. Hen, L. Weinstein, E. Piasetzky, and H. Hakobyan, *In Medium Proton Structure Functions, SRC, and the EMC effect, Jefferson Lab experiment E12-11-003A* (2015).

[35] E. Braaten, in *The BCS-BEC Crossover and the Unitary Fermi Gas*, edited by W. Zwerger (Springer, Berlin, 2012).

[36] J. T. Stewart, J. P. Gaebler, T. E. Drake, and D. S. Jin, Phys. Rev. Lett. **104**, 235301 (2010).

[37] Z. Ye, Ph.D. thesis, University of Virginia (2013), 1408.5861.

[38] M. Vanhalst, W. Cosyn, and J. Ryckebusch, Phys. Rev. C **84**, 031302 (2011), URL http://link.aps.org/doi/10.1103/PhysRevC.84.031302.

[39] M. Vanhalst, J. Ryckebusch, and W. Cosyn, Phys. Rev. C **86**, 044619 (2012).

[40] J. Ryckebusch, M. Vanhalst, and W. Cosyn, Journal of Physics G: Nuclear and Particle Physics **42**, 055104 (2015), 1405.3814, URL http://stacks.iop.org/0954-3899/42/i=5/a=055104.

[41] R. B. Wiringa, R. Schiavilla, S. C. Pieper, and J. Carlson, Phys. Rev. C **89**, 024305 (2014).

[42] C. Colle, O. Hen, W. Cosyn, I. Korover, E. Piasetzky, J. Ryckebusch, and L. B. Weinstein, Phys. Rev. C **92**, 024604 (2015).

[43] J. Kelly, Adv. Nucl. Phys. **23**, 75 (1996).

[44] T. De Forest, Nucl. Phys. **A392**, 232 (1983).

[45] M. Sargsian, *Private communication*.

[46] F. Benmokhtar et al. (Jefferson Lab Hall A Collaboration), Phys. Rev. Lett. **94**, 082305 (2005).

[47] O. Hen et al. (CLAS Collaboration), Phys.Lett. **B722**, 63 (2013), 1212.5343.

[48] K. Garrow, D. McKee, A. Ahmidouch, C. S. Armstrong, J. Arrington, R. Asaturyan, S. Avery, O. K. Baker, D. H. Beck, H. P. Blok, et al., Phys. Rev. C **66**, 044613 (2002), URL http://link.aps.org/doi/10.1103/PhysRevC.66.044613.

[49] K. Fissum et al. (Jefferson Lab Hall A Collaboration), Phys.Rev. **C70**, 034606 (2004), nucl-ex/0401021.

[50] J. Gao et al., Phys. Rev. Lett. **84**, 3265 (2000).

[51] N. Liyanage, B. D. Anderson, K. A. Aniol, L. Auerbach, F. T. Baker, J. Berthot, W. Bertozzi, P.-Y. Bertin, L. Bimbot, W. U. Boeglin, et al. (The Jefferson Lab Hall A Collaboration), Phys. Rev. Lett. **86**, 5670 (2001), URL http://link.aps.org/doi/10.1103/PhysRevLett.86.5670.

[52] J. Herraiz, Ph.D. thesis, Universidad Complutense de Madrid (2010).

[53] D. Dutta et al., Phys. Rev. C **68**, 064603 (2003), URL http://link.aps.org/doi/10.1103/PhysRevC.68.064603.

[54] J. Arrington, D. Higinbotham, G. Rosner, and M. Sargsian, Prog.Part.Nucl.Phys. **67**, 898 (2012), 1104.1196.

[55] M. M. Rvachev et al. (Jefferson Lab Hall A Collaboration), Phys. Rev. Lett. **94**, 192302 (2005).

[56] D. Rohe, O. Benhar, C. S. Armstrong, R. Asaturyan, O. K. Baker, S. Bueltmann, C. Carasco, D. Day, R. Ent, H. C. Fenker, et al. (E97-006 Collaboration), Phys. Rev. C **72**, 054602 (2005), URL http://link.aps.org/doi/10.1103/PhysRevC.72.054602.

[57] D. Rohe, C. S. Armstrong, R. Asaturyan, O. K. Baker, S. Bueltmann, C. Carasco, D. Day, R. Ent, H. C. Fenker, K. Garrow, et al. (E97-006 Collaboration), Phys. Rev. Lett. **93**, 182501 (2004), URL http://link.aps.org/doi/10.1103/PhysRevLett.93.182501.

[58] O. Hen, H. Hakobyan, R. Shneor, E. Piasetzky, L. Weinstein, W. Brooks, S. M.-T. Beck, S. Gilad, I. Korover, A. Beck, et al., Physics Letters B **722**, 63 (2013), ISSN 0370-2693, URL http://www.sciencedirect.com/science/article/pii/S03702693130%02906.

[59] P. Monaghan, R. Shneor, R. Subedi, B. D. Anderson, K. Aniol, J. Annand, J. Arrington,

H. B. Benaoum, F. Benmokhtar, P. Bertin, et al., Journal of Physics G: Nuclear and Particle Physics **41**, 105109 (2014), URL http://stacks.iop.org/0954-3899/41/i=10/a=105109.

[60] R. Shneor et al., Phys. Rev. Lett. **99**, 072501 (2007).

[61] C. Colle, W. Cosyn, and J. Ryckebusch, *Final-state interactions in two-nucleon knockout reactions* (2015), 1512.07841.